

# Rapidly sheared homogeneous stratified turbulence in a rotating frame

S. C. Kassinos,<sup>a)</sup> E. Akylas,<sup>b)</sup> and C. A. Langer

Department of Mechanical and Manufacturing Engineering, University of Cyprus, 75 Kallipoleos, Nicosia 1678, Cyprus

(Received 25 October 2006; accepted 26 January 2007; published online 23 February 2007)

Rapid distortion theory is applied to stratified homogeneous turbulence that is sheared in a rotating frame. Insight into the stabilizing and destabilizing effects of the combined stratification and frame rotation is gained by considering initial fields that are two-dimensional, with the axis of independence aligned with the flow direction. For these conditions, we derive solutions for the Fourier components of the flow variables, and for one-point statistics in physical space. The analytical results are in qualitative agreement with the exact numerical solution for initially isotropic homogeneous turbulence, and they could be a reference point for the development of turbulence models. © 2007 American Institute of Physics. [DOI: 10.1063/1.2710291]

Rapid distortion theory (RDT) has been widely used in studying the effects of rotation or stratification in sheared turbulence.<sup>1–5</sup> In this study, we use RDT to examine the combined effects of rotation and stratification in the case of stratified turbulence that is sheared in a rotating frame (Fig. 1). The analysis carried out herein leads to analytical expressions for the asymptotic states of the Reynolds stress and structure tensors, and these can then be used in the development of closures such as the algebraic structure-based model.<sup>6</sup> The studied case is of relevance to turbomachinery flows (for example, with internal blade cooling passages) and to geophysical flows (for example, the flow over a hill or bump). Most recently, a connected work has been studied by Salhi and Cambon,<sup>7</sup> where the rotation was aligned with the vertical direction. Under inviscid RDT and using the Boussinesq approximation, the transport equations for the fluctuating velocity and density components  $u_i$  and  $\rho$  become

$$\begin{aligned} \frac{\partial u_i}{\partial t} + Sx_2 \frac{\partial u_i}{\partial x_1} &= -\delta_{i1}Su_2 - \frac{1}{\rho_0} \frac{\partial p}{\partial x_i} - \frac{\rho}{\rho_0} g \delta_{i2} + 2\varepsilon_{ij3}\Omega^f u_j, \\ \frac{\partial \rho}{\partial t} + Sx_2 \frac{\partial \rho}{\partial x_1} &= -Hu_2, \end{aligned} \quad (1)$$

where  $S=dU_1/dx_2$  is the mean velocity gradient,  $\Omega^f$  is the frame rotation rate,  $g$  is the gravitational constant,  $\rho_0$  is the reference density, and  $H=d\bar{p}/dx_2$  is the mean density gradient. We consider an initially three-component (3C) but two-dimensional (2D) turbulence, independent of the flow direction  $x_1$ , with  $u_i=u_i(x_2, x_3)$  for  $i=1, 2, 3$ . Because the chosen axis of independence is aligned with flow direction, it does not become tilted at later times. As a result, the momentum and density equations (1) simplify to

$$\begin{aligned} \partial u_i / \partial t &= -\delta_{i1}Su_2 - (\partial p / \partial x_i + \rho g \delta_{i2}) / \rho_0 + 2\varepsilon_{ij3}\Omega^f u_j, \\ \partial \rho / \partial t &= -u_2 H. \end{aligned} \quad (2)$$

The vanishing of the convective terms means that Fourier expansion methods can be used without the need to trans-

form coordinates into a frame deforming with the mean flow, and thus we obtain the following set of evolution equations for the Fourier coefficients:

$$\begin{aligned} \frac{\partial \hat{u}_1}{\partial \beta} &= -(1-\eta)\hat{u}_2, \quad \frac{\partial \hat{u}_2}{\partial \beta} = -\eta n_3^2 \hat{u}_1 - \frac{\hat{\rho} g n_3^2}{S\rho_0}, \\ \frac{\partial \hat{u}_3}{\partial \beta} &= \eta n_3 n_3 \hat{u}_1 - \frac{\hat{\rho} g n_3 n_3}{S\rho_0}, \quad \frac{\partial \hat{\rho}}{\partial \beta} = -\frac{H}{S} \hat{u}_2, \end{aligned} \quad (3)$$

where  $\beta=St$  is the total shear,  $\eta=2\Omega^f/S$  is the dimensionless rotation rate, and  $n_i=k_i/k$  are the relative values of the components of the wave-number vector, whose magnitude is  $k=\sqrt{k_i k_i}$ . Differentiating (3) with respect to  $\beta$ , we obtain

$$\partial^2 \hat{u}_2 / \partial \beta^2 = Zn_3^2 \hat{u}_2, \quad \partial^2 \hat{u}_3 / \partial \beta^2 = Zn_3^2 \hat{u}_3. \quad (4)$$

In the above,  $Z=B-\text{Ri}_g$ , where  $B=\eta(1-\eta)$  is the Bradshaw<sup>8</sup>–Pedley<sup>9</sup> stability parameter, and  $\text{Ri}_g=-Hg/S^2\rho_0$  is the Richardson number. Clearly the solution of (3) and (4) depends on the value of  $Z$ . As will be shown, positive values of this parameter correspond to unstable cases, resulting in an exponential turbulent kinetic energy (TKE) growth, while negative values cause a stabilizing behavior. Regarding the stabilizing criterion, a similar result can also be correctly obtained using a simplified 1D pressureless analysis (Brethouwer<sup>10</sup>). The general solution for the Fourier transformed density and velocity components (3) and (4) yields

$$\begin{aligned} \hat{u}_1 &= \left[ -\frac{\text{Ri}_g}{Z} + \frac{Z+\text{Ri}_g}{Z} \cosh(\sqrt{Z}n_3\beta) \right] \hat{u}_1^0 \\ &\quad - \frac{(1-\eta)\sinh(\sqrt{Z}n_3\beta)}{\sqrt{Z}n_3} \hat{u}_2^0, \\ \hat{u}_2 &= \cosh(\sqrt{Z}n_3\beta) \hat{u}_2^0 - \frac{\eta n_3}{\sqrt{Z}} \sinh(\sqrt{Z}n_3\beta) \hat{u}_1^0, \\ \hat{u}_3 &= \cosh(\sqrt{Z}n_3\beta) \hat{u}_3^0 + \frac{\eta n_2}{\sqrt{Z}} \sinh(\sqrt{Z}n_3\beta) \hat{u}_1^0, \\ \hat{\rho} - \hat{\rho}^0 &= \left[ -\frac{H\eta}{SZ} + \frac{H\eta}{SZ} \cosh(\sqrt{Z}n_3\beta) \right] \hat{u}_1^0 - \frac{H \sinh(\sqrt{Z}n_3\beta)}{S\sqrt{Z}n_3} \hat{u}_2^0. \end{aligned} \quad (5)$$

In the above relations, the superscript 0 is used in order to denote initial values. Calculating the velocity spectra

<sup>a)</sup>Also at the Center for Turbulence Research, Stanford University/NASA-Ames, Stanford, CA 94305. Electronic mail: kassinos@ucy.ac.cy

<sup>b)</sup>Also at the Institute of Environmental Research, National Observatory of Athens, Greece.

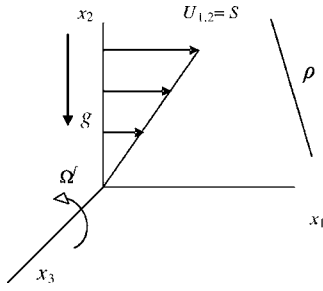


FIG. 1. Illustration of the general case for stratified homogeneous turbulence that is sheared in a rotating frame.

$E_{ij} \sim \overline{\hat{u}_i \hat{u}_j^*}$ , we integrate over all the wave numbers to obtain analytical expressions in physical space for the development of the stress components  $R_{ij} = u_i u_j = \iint E_{ij} d^3 \mathbf{k}$  and the structure dimensionality tensor components<sup>1,2</sup>  $D_{ij} = \iint E_{mn}(\mathbf{k}) k_i k_j / k^2 d^3 \mathbf{k}$ . The combined use of these two tensors gives a description of the morphology of turbulent fields.<sup>1</sup> In the following, we present solutions in physical space for two different initializations, vortical 2D-2C and jetal 2D-1C (for an explanation of vortical and jetal initial conditions, see Ref. 1). Because of the linearity of the governing equations, the solutions corresponding to initially jetal 2D-1C and to initially vortical 2D-2C cases can be superimposed. This way, evolution histories for  $R_{ij}$ ,  $D_{ij}$  and fluxes can be generated for various 2D-3C initial fields consisting of uncorrelated jets and vortices. In the case of an initially 2D-2C vortical velocity spectrum (see also Cambon *et al.*<sup>11</sup>),

$$E_{ij}^{vor}(k, 0) = \frac{E(k)}{2\pi k} \delta(k_1) \left( \delta_{ij} - \frac{k_i k_j}{k^2} - \delta_{i1} \delta_{j1} \right),$$

$$i = 1, 2, 3 \quad j = 1, 2, 3, \quad (6)$$

the Reynolds stress components become

$$R_{11}^{vor}/q_0^2 = (1 - \eta)^2 [-1 + I_0(2\sqrt{Z}\beta)]/(2Z),$$

$$R_{22}^{vor}/q_0^2 = [1 + 2I_0(2\sqrt{Z}\beta) - I_1(2\sqrt{Z}\beta)/(\sqrt{Z}\beta)]/4,$$

$$R_{33}^{vor}/q_0^2 = [1 + I_1(2\sqrt{Z}\beta)/(\sqrt{Z}\beta)]/4,$$

$$R_{12}^{vor}/q_0^2 = -(1 - \eta)I_1(2\sqrt{Z}\beta)/(2\sqrt{Z}),$$

where  $I_n$  are Bessel functions of the first kind and  $q_0^2$  is twice the initial TKE. From (7) it can be shown that the turbulent kinetic energy evolves with time as

$$q_{vor}^2/q_0^2 = [Z - (1 - \eta)^2 + (1 - \text{Ri}_g - \eta)I_0(2\sqrt{Z}\beta)]/2Z. \quad (8)$$

When  $Z > 0$ , Eq. (9) approaches an exponential growth for large total shear,

$$\lim_{\beta \rightarrow \infty} q_{vor}^2(Z > 0)/q_0^2 = (1 - \text{Ri}_g - \eta) \exp(2\sqrt{Z}\beta)/(4\sqrt{\pi}Z^{5/4}\beta^{1/2}). \quad (9)$$

On the other hand, when  $Z < 0$ ,  $\sqrt{Z}$  is imaginary and the term on the right-hand side of (8) becomes  $I_0(2\sqrt{Z}\beta) = J_0(2\sqrt{-Z}\beta)$ , where  $J_n$  are Bessel functions of the second

kind. Thus, the turbulent kinetic energy stabilizes, showing decreasing oscillations around the value

$$\lim_{\beta \rightarrow \infty} q_{vor}^2(Z < 0)/q_0^2 = 1/2 - (1 - \eta)^2/2Z. \quad (10)$$

At the neutral limit  $Z=0$ , the TKE evolution becomes a quadratic function of time

$$\lim_{Z \rightarrow 0} q_{vor}^2/q_0^2 = 1 + (1 - \text{Ri}_g - \eta)\beta^2/2. \quad (11)$$

The dimensionality tensor components for this vortical initialization are

$$D_{11}^{vor}/q_0^2 = 0, \quad D_{22}^{vor}/q_0^2 = [Z + (1 - \eta)^2][1/2 + I_1(2\sqrt{Z}\beta)/2\sqrt{Z}\beta]/2Z - (1 - \eta)^2/2Z,$$

$$D_{33}^{vor}/q_0^2 = [Z + (1 - \eta)^2][1/2 + I_0(2\sqrt{Z}\beta) - I_1(2\sqrt{Z}\beta)/2\sqrt{Z}\beta]/2Z - (1 - \eta)^2/2Z. \quad (12)$$

From Eqs. (7)–(12), we may calculate the normalized values of the Reynolds stress,  $r_{ij} = R_{ij}/R_{kk}$ , and the structure dimensionality tensor,  $d_{ij} = D_{ij}/R_{kk}$ , in order to describe the states of the turbulence.<sup>1</sup> When  $Z > 0$ , the asymptotic limits of these forms for large total shear become

$$\lim_{\beta \rightarrow \infty} r_{11} = \frac{(1 - \eta)^2}{1 - \eta - \text{Ri}_g}, \quad \lim_{\beta \rightarrow \infty} r_{22} = \frac{Z}{1 - \eta - \text{Ri}_g},$$

$$\lim_{\beta \rightarrow \infty} r_{12} = \frac{-(1 - \eta)Z^{1/2}}{1 - \eta - \text{Ri}_g}, \quad \lim_{\beta \rightarrow \infty} d_{33} = 1, \quad (13)$$

corresponding to a 1D-2C state where all the dependence is confined along the axis of the frame rotation ( $x_3$ ), and the distribution of the energy in the plane normal to that axis depends on the actual values of  $\eta$  and  $\text{Ri}_g$ . Such a state corresponds to sheets extending perpendicular to the axis of the frame rotation and to a turbulent motion aligned with the other two directions.

For the stable cases in which  $Z < 0$ ,

$$\lim_{\beta \rightarrow \infty} r_{11} = \frac{-(1 - \eta)^2}{Z - (1 - \eta)^2},$$

$$\lim_{\beta \rightarrow \infty} r_{22} = \lim_{\beta \rightarrow \infty} r_{33} = \frac{Z/2}{Z - (1 - \eta)^2}, \quad (14)$$

$$\lim_{\beta \rightarrow \infty} r_{12} = 0, \quad \lim_{\beta \rightarrow \infty} d_{22} = \lim_{\beta \rightarrow \infty} d_{33} = 1/2,$$

where the mean shear drives 2D-2C initially vortical turbulence to a 2D-3C state with axisymmetric structures and an equipartition of energy within the plane normal to the axis of the mean flow. The final partition of the TKE along the axis of independence (i.e.,  $r_{11}$ ) and normal to the axis (i.e.,  $r_{22}, r_{33}$ ) depends on the values of  $\eta$  and  $Z$ . Finally, for the neutral cases corresponding to  $Z=0$  (apart from the limiting case with  $\eta=1$  and  $\text{Ri}_g=0$ , where the turbulence remains constant equal to its initial state), the asymptotic limits for  $r_{ij}$  and  $d_{ij}$  are

$$\lim_{\beta \rightarrow \infty} r_{11} = 1, \quad \lim_{\beta \rightarrow \infty} r_{12} = 0, \quad \lim_{\beta \rightarrow \infty} d_{22} = 1/4, \quad \lim_{\beta \rightarrow \infty} d_{33} = 3/4. \quad (15)$$

This means that the initially 2D vortical turbulence is driven to jetal turbulence with eddies flattened along the  $x_3$  axis.

When the turbulence is initialized using a 1C-2D jetal velocity spectrum tensor

$$E_{ij}^{\text{jet}}(k, 0) = E(k) \delta(k_1) \delta_{i1} \delta_{j1} / 2\pi k, \quad i = 1, 2, 3 \quad j = 1, 2, 3, \quad (16)$$

the Reynolds stresses are calculated as

$$\begin{aligned} R_{11}^{\text{jet}}/q_0^2 &= \text{Ri}_g^2/Z^2 - 2(Z\text{Ri}_g + \text{Ri}_g^2)I_0(\sqrt{Z}\beta)/Z^2 \\ &\quad + (Z + \text{Ri}_g)^2[1 + I_0(2\sqrt{Z}\beta)]/2Z^2, \\ R_{22}^{\text{jet}}/q_0^2 &= \eta^2[-1 + 2I_0(2\sqrt{Z}\beta) - I_1(2\sqrt{Z}\beta)/(\sqrt{Z}\beta)]/(4Z), \\ R_{33}^{\text{jet}}/q_0^2 &= \eta^2[-1 + I_1(2\sqrt{Z}\beta)/(\sqrt{Z}\beta)]/(4Z), \\ R_{12}^{\text{jet}}/q_0^2 &= \eta[2\text{Ri}_g I_1(\sqrt{Z}\beta) - (Z + \text{Ri}_g)I_1(2\sqrt{Z}\beta)]/2Z^{3/2}. \end{aligned} \quad (17)$$

The trace in this jetal case evolves as

$$\begin{aligned} \frac{q_{\text{jet}}^2}{q_0^2} &= \frac{\text{Ri}_g^2}{Z^2} - 2\frac{Z\text{Ri}_g + \text{Ri}_g^2}{Z^2}I_0(\sqrt{Z}\beta) + \frac{(Z + \text{Ri}_g)^2}{Z^2} \frac{1 + I_0(2\sqrt{Z}\beta)}{2} \\ &\quad + \frac{\eta^2 - 1 + I_0(2\sqrt{Z}\beta)}{Z}, \end{aligned} \quad (18)$$

and, similarly to the vortical case, when  $Z > 0$  it grows exponentially at large total shear,

$$\lim_{\beta \rightarrow \infty} q_{\text{jet}}^2/q_0^2 = [(Z + \text{Ri}_g)^2/Z + \eta^2] \exp(2\sqrt{Z}\beta)/(4\sqrt{\pi}Z^{5/4}\beta^{1/2}). \quad (19)$$

When  $Z < 0$ , the TKE stabilizes, showing decreasing oscillations around the value

$$\lim_{\beta \rightarrow \infty} q_{\text{jet}}^2/q_0^2 = [2\text{Ri}_g^2 + (Z + \text{Ri}_g)^2 - \eta^2 Z]/2Z^2, \quad (20)$$

while at the neutral limit  $Z=0$ , the TKE evolves as a quartic polynomial,

$$\lim_{Z \rightarrow 0} q_{\text{jet}}^2/q_0^2 = 1 + (\eta^2 + \text{Ri}_g)\beta^2/2 + 3\text{Ri}_g^2\beta^4/32 \quad (21)$$

depending mainly on the value of  $\text{Ri}_g$ . It has to be pointed out, however, that in the case of the jetal initialization with no frame rotation ( $\eta=0$ ), the turbulence remains unmodified, as can be shown from Eqs. (18)–(21). This differs from the corresponding behavior in the vortical initialization. The dimensionality tensor is

$$D_{11}^{\text{jet}}/q_0^2 = 0,$$

$$\begin{aligned} \frac{D_{22}^{\text{jet}}}{q_0^2} &= \frac{\text{Ri}_g^2}{2Z^2} - \frac{\eta^2}{Z} + \frac{(\text{Ri}_g + Z)^2 + \eta^2 Z}{2Z^2} \left[ \frac{1}{2} + \frac{I_1(2\sqrt{Z}\beta)}{2\sqrt{Z}\beta} \right] \\ &\quad - \frac{2(\text{Ri}_g^2 + Z\text{Ri}_g)}{Z^2} \frac{I_1(\sqrt{Z}\beta)}{\sqrt{Z}\beta}, \\ \frac{D_{33}^{\text{jet}}}{q_0^2} &= \frac{\text{Ri}_g^2}{2Z^2} + \frac{(\text{Ri}_g + Z)^2 + \eta^2 Z}{2Z^2} \left[ \frac{1}{2} + I_0(2\sqrt{Z}\beta) - \frac{I_1(2\sqrt{Z}\beta)}{2\sqrt{Z}\beta} \right] \\ &\quad - \frac{2(\text{Ri}_g^2 + Z\text{Ri}_g)}{Z^2} \left[ I_0(\sqrt{Z}\beta) - \frac{I_1(\sqrt{Z}\beta)}{\sqrt{Z}\beta} \right]. \end{aligned} \quad (22)$$

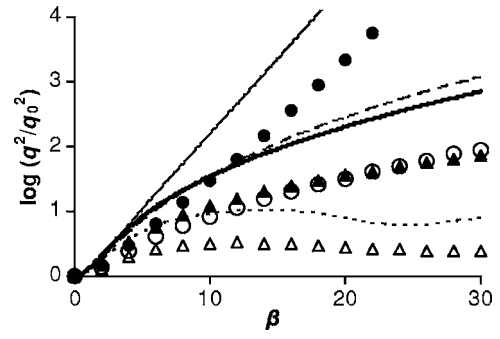


FIG. 2. Evolution of the TKE for the cases with  $\eta=0.2$  and  $\text{Ri}_g$  equal to 0.08 (unstable: thin continuous, solid circles), 0.16 (neutral: long dashed, open circles), 0.24 (stable: short dashed, open triangles), as well as the case with  $\eta=-0.1$  and  $\text{Ri}_g=-0.11$  (neutral: bold continuous, solid triangles) calculated from the 3D initially isotropic exact PRM numerical solution (symbols) and the 2D analytical solution with  $k_1=0$  (lines).

For  $Z > 0$ , the normalized values of the stresses  $r_{ij}$  and the structure dimensionality tensor components  $d_{ij}$  reach exactly the same asymptotic values as given by (13), and thus correspond to the same 1D-2C state that has been found for the vortical case. For the stable cases, characterized by  $Z < 0$ , shear drives turbulence to a 2D-3C state

$$\begin{aligned} \lim_{\beta \rightarrow \infty} r_{11} &= \frac{2\text{Ri}_g^2 + (Z + \text{Ri}_g)^2}{2\text{Ri}_g^2 + (Z + \text{Ri}_g)^2 - \eta^2 Z}, \\ \lim_{\beta \rightarrow \infty} r_{22} &= \lim_{\beta \rightarrow \infty} r_{33} = \frac{-\eta^2 Z/2}{2\text{Ri}_g^2 + (Z + \text{Ri}_g)^2 - \eta^2 Z}, \\ \lim_{\beta \rightarrow \infty} r_{12} &= 0, \quad \lim_{\beta \rightarrow \infty} d_{11} = 0, \quad \lim_{\beta \rightarrow \infty} d_{22} = \lim_{\beta \rightarrow \infty} d_{33} = 1/2, \end{aligned} \quad (23)$$

showing an equipartition of energy within the plane normal to the axis of the mean flow, similarly to the vortical initialization. However, the final partition of the TKE along the axis of independence (i.e.,  $r_{11}$ ) and normal to the axis (i.e.,  $r_{22}, r_{33}$ ) is different compared to (14). For  $Z=0$ , the initially 2D-1C jetal turbulence remains jetal with eddies flattened along the  $x_3$  axis,

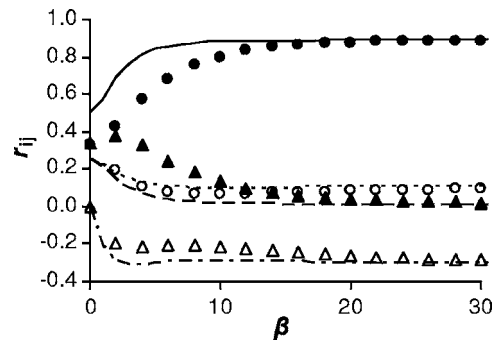
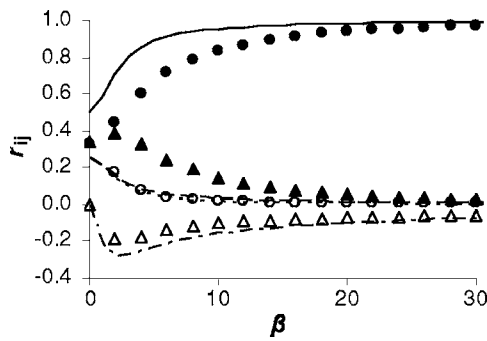
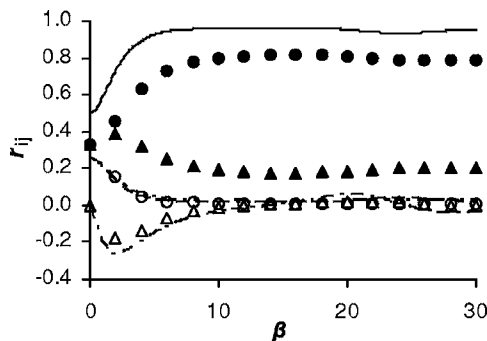
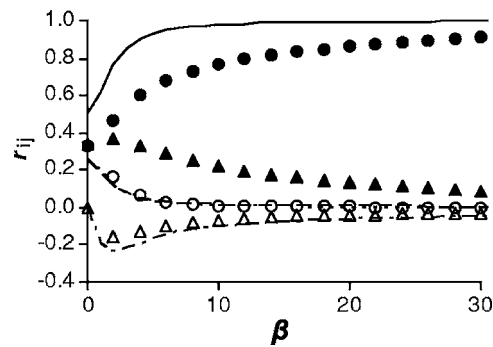


FIG. 3. Evolution of the normalized stress components 11 (continuous, solid circles), 22 (short dashed, open circles), 33 (long dashed, solid triangles), and 12 (dotted dashed, open triangles) calculated from the 3D initially isotropic exact PRM numerical solution (symbols) and the 2D analytical solution with  $k_1=0$  (lines) presented here, for the unstable case with  $\eta=0.2$ ,  $\text{Ri}_g=0.08$  and  $Z=0.08$ .

FIG. 4. As in Fig. 3, for the neutral case with  $\eta=0.2, Ri_g=0.16$  and  $Z=0$ .

$$\lim_{\beta \rightarrow \infty} r_{11} = 1, \quad \lim_{\beta \rightarrow \infty} r_{12} = 0, \quad \lim_{\beta \rightarrow \infty} d_{22} = 1/6, \quad \lim_{\beta \rightarrow \infty} d_{33} = 5/6. \quad (24)$$

In Fig. 2, we present a comparison between the TKE evolution calculated by the analytical expressions derived here, for an equally weighted (50%-50%) superposition between the vortical and the jetal initializations, and the numerical solution of the 3D-3C initially isotropic initialization calculated using the particle representation model (PRM) developed by Kassinos and Reynolds,<sup>12</sup> with large enough numbers of particles to ensure the accuracy of the solution. From the comparison, it turns out that the 2D approach, although overestimating the TKE, explains accurately the type (algebraic or exponential) of the TKE growth, while identifying  $Z$  as the principal parameter for the determination of the stability of the turbulent flow. Starting with the unstable case with  $\eta = 0.2$  and  $Ri_g = 0.08$ , we notice the profound exponential evolution with time. An increase of  $Ri_g$  to 0.16, resulting in  $Z = 0$ , causes a departure from the exponential toward a polynomial growth, while a further increase of  $Ri_g$  to 0.24 stabilizes the TKE. Also, a combination of  $\eta = -0.1$  (which tends to stabilize) and  $Ri_g = -0.11$  (which tends to destabilize the TKE) resulting in  $Z = 0$  again produces a neutral, polynomial growth of the TKE with time. In Figs. 3–6, the evolutions of the normalized stress components  $r_{ij}$  are illustrated for all the above-mentioned cases, and compared with the respective 3D-PRM exact numerical solutions. As can be seen for the neutral and the unstable cases, the limiting states reached by the analytical 2D solution are in good agreement with the

FIG. 5. As in Fig. 3, for the stable case with  $\eta=0.2, Ri_g=0.24$  and  $Z=-0.08$ .FIG. 6. As in Fig. 3, for the neutral case with  $\eta=-0.1, Ri_g=-0.11$  and  $Z=0$ .

corresponding limiting states obtained numerically (PRM) for initially 3D isotropic turbulence. The same agreement can be drawn for  $d_{ij}$  (not shown here), where, for the unstable and the neutral regimes, the  $d_{11}$  component (initially isotropic case) tends quickly to zero, especially in the unstable cases. In contrast, when  $Z < 0$ , the initially 3D character of the turbulence becomes more important. As a result, the limiting states reached by the analytical 2D solution start to diverge from the numerical 3D results (Fig. 5). In spite of the moderate disagreement in the tensor components, both initializations result in the stabilization of the TKE, as appropriate.

This work has been performed under the UCY-CompSci project, a Marie Curie Transfer of Knowledge (TOK-DEV) grant (Contract No. MTKD-CT-2004-014199) and under the WALLTURB project (a European synergy for the assessment of wall turbulence, Contract No. AST4-CT-2005-516008), both funded by the CEC under the 6th framework program.

- <sup>1</sup>S. C. Kassinos, W. C. Reynolds, and M. M. Rogers, "One-point turbulence structure tensors," *J. Fluid Mech.* **428**, 213 (2001).
- <sup>2</sup>E. Akylas, S. C. Kassinos, and C. A. Langer, "Analytical solution for a special case of rapidly distorted turbulent flow in a rotating frame," *Phys. Fluids* **18**, 085104 (2006).
- <sup>3</sup>A. Salhi and C. Cambon, "An analysis of rotating shear flow using linear theory and DNS and LES results," *J. Fluid Mech.* **347**, 171 (1997).
- <sup>4</sup>A. Salhi, "Similarities between rotation and stratification effects on homogeneous shear flow," *Theor. Comput. Fluid Dyn.* **15**, 339 (2002).
- <sup>5</sup>H. Hanazaki and J. C. R. Hunt, "Structure of unsteady stably stratified turbulence with mean shear," *J. Fluid Mech.* **507**, 1 (2004).
- <sup>6</sup>S. C. Kassinos, C. A. Langer, G. Kalitzin, and G. Iaccarino, "A simplified structure-based model using standard turbulence scale equations: Computation of rotating wall-bounded flows," *Int. J. Heat Fluid Flow* **27**, 653 (2006).
- <sup>7</sup>A. Salhi and C. Cambon, "Advances in rapid distortion theory: From rotating shear flows to the baroclinic instability," *J. Appl. Mech.* **73**, 449 (2006).
- <sup>8</sup>P. Bradshaw, "The analogy between streamline curvature and buoyancy in turbulent shear flow," *J. Fluid Mech.* **36**, 177 (1969).
- <sup>9</sup>T. Pedley, "On the stability of viscous flows in a rapidly rotating pipe," *J. Fluid Mech.* **35**, 97 (1969).
- <sup>10</sup>G. Brethouwer, "The effect of rotation on rapidly sheared homogeneous turbulence and passive scalar transport. Linear theory and direct numerical simulation," *J. Fluid Mech.* **542**, 305 (2005).
- <sup>11</sup>C. Cambon, N. N. Mansour, and F. S. Godeferd, "Energy transfer in rotating turbulence," *J. Fluid Mech.* **337**, 303 (1997).
- <sup>12</sup>S. C. Kassinos and W. C. Reynolds, "A particle representation model for the deformation of homogeneous turbulence," *Annual Research Briefs 1996*, Stanford University and NASA Ames Research Center: Center for Turbulence Research (1996), pp. 31–50.